

# Oceanic mesoscale cyclones cluster surface Lagrangian material

Clément Vic<sup>1</sup>, Solenne Hascoët<sup>1</sup>, Jonathan Gula<sup>1,2</sup>, Thierry Huck<sup>1</sup>, and Christophe Maes<sup>1</sup>

<sup>1</sup>Laboratoire d'Océanographie Physique et Spatiale, Univ. Brest, CNRS, IRD, Ifremer, Plouzané, France  
<sup>2</sup>Institut Universitaire de France (IUF), Paris, France

## Key Points:

- Surface Velocity Program drifters are preferentially trapped into mesoscale cyclones rather than in anticyclones
- Lagrangian analysis of a mesoscale-resolving simulation shows that particles cluster preferentially in cyclonic fronts and eddies
- Particles cluster in cyclonic regions a few days before the formation and detection of mesoscale cyclones

14 **Abstract**

15 An asymmetry in the clustering of oceanic surface material has been observed at the sub-  
 16 mesoscales. Energetic and ephemeral submesoscale cyclonic fronts are associated with  
 17 convergence zones, hence cluster surface material. Their anticyclonic counterparts do not  
 18 feature such effect. Yet, at the mesoscale, literature has been contradictory about such  
 19 an asymmetry. Here, we combine surface drifter trajectories with an altimetry-derived  
 20 mesoscale eddy database in the North Atlantic to show that mesoscale cyclones contain  
 21 24% more drifters than anticyclones. A numerical Lagrangian experiment using a mesoscale-  
 22 resolving model quantitatively reproduces the observational results. It reveals that par-  
 23 ticles preferentially cluster in cyclonic regions, both in fronts and eddies. The model fur-  
 24 ther suggests that ageostrophic cyclonic fronts concentrate particles a few days before  
 25 the eddy formation and detection.

26 **1 Introduction**

27 Mesoscale eddies are ubiquitous features in the oceans and dominate the kinetic  
 28 energy reservoir. They mostly arise from instabilities of large-scale persistent currents  
 29 and have been routinely observed through satellite altimetry for almost three decades  
 30 (Chelton et al., 2011). They play an active role in the transport of tracers, yet several  
 31 questions on the underlying mechanisms of dispersion and their regional and global im-  
 32 plications remain debated (e.g., Zhang et al., 2014; Abernathey & Haller, 2018).

33 As put forward in McWilliams (2008), “almost all our understanding of eddy dy-  
 34 namics and phenomena has its roots in quasi-geostrophic theory”. Indeed, the dominant  
 35 instabilities of large-scale currents and the lifecycle of mesoscale eddies are well described  
 36 by the quasi-geostrophic theory. This theory relies on several assumptions, a fundamen-  
 37 tal one being that the Rossby number of the flow ( $Ro$ ), which compares the inertial force  
 38 to the Coriolis force, is small ( $Ro < 0.1$ , e.g., section 5.3 in Vallis, 2006). In the limit  
 39 of  $Ro \rightarrow 0$ , there is a perfect symmetry in the phenomenology of cyclones and anticy-  
 40 clones. For  $Ro = O(0.1)$ , an asymmetry is observed to develop with a dominance of an-  
 41 ticyclones over cyclones. Correspondingly, the probability density function of the rela-  
 42 tive vorticity of the flow is slightly skewed towards negative values (e.g., Polvani et al.,  
 43 1994). Reasons for this dominance are manifold (see the discussion in Polvani et al., 1994),  
 44 but the sole kinematic consequence of the emergence of inertial forces is the acceleration  
 45 of anticyclones and the slowing down of cyclones (Penven et al., 2014). No further kine-  
 46 matic asymmetry emerges from the regime of  $Ro = O(0.1)$ .

47 Two mechanisms commonly invoked to explain asymmetrical effects in convergence  
 48 and divergence in cyclones and anticyclones are *eddy pumping* and *Ekman pumping* (McGillicuddy Jr,  
 49 2016). The former is active towards the beginning and the end of the eddy life cycle (e.g.,  
 50 Figure 4.21 in Flierl & McGillicuddy, 2002). When a surface-intensified eddy forms, isopy-  
 51 cnals in the thermocline are pumped up (down) in cyclones (anticyclones), hence result-  
 52 ing in a divergence (convergence) of surface horizontal velocity in cyclones (anticyclones).  
 53 The opposite happens when the eddy decays. The second mechanism – Ekman pump-  
 54 ing (Gaube et al., 2015) – results from a differential wind stress on the upwind and down-  
 55 wind sides of the eddy, which creates a horizontal convergence (divergence) of Ekman  
 56 transport in cyclones (anticyclones).

57 The oceanic surface boundary layer is host to a submesoscale regime of turbulence,  
 58 where  $Ro$  reaches  $O(1)$  values and the quasi-geostrophic regime does not hold. In this  
 59 regime, vorticity is skewed towards positive values, and a clear dominance of cyclonic ed-  
 60 dies and fronts has been observed and modelled (Rudnick, 2001; Roullet & Klein, 2010;  
 61 Shcherbina et al., 2013; Buckingham et al., 2016). There is growing evidence in litera-  
 62 ture that submesoscale cyclonic vorticity is associated with convergence zones, both from  
 63 Eulerian (Shcherbina et al., 2013) and Lagrangian observations (D’Asaro et al., 2018;

64 Esposito et al., 2021). Theory and numerical modelling corroborate these observations  
 65 (Barkan et al., 2019; Balwada et al., 2021).

66 We now elaborate on the Lagrangian implications of the mesoscale and submesoscale  
 67 regimes of turbulence. If the mesoscale eddy field is ruled by a quasi-geostrophic regime,  
 68 there should be an equipartition of Lagrangian material into mesoscale cyclones and an-  
 69 ticyclones, stemming from their kinematic symmetry. However, it is tempting to extrap-  
 70 olate on the efficiency of submesoscale cyclonic flows to cluster material to test the hy-  
 71 pothesis that an upscaling effect – compatible with an inverse cascade of turbulence in  
 72 surface quasi-geostrophic flows (Capet et al., 2008) – could lead to a preferred accumu-  
 73 lation of Lagrangian material into mesoscale cyclones. Submesoscales are ephemeral and  
 74 difficult to observe but mesoscale eddies are easily tracked by satellite altimetry, so a po-  
 75 tential asymmetry between the trapping capacity of cyclones and anticyclones could help  
 76 to refine our understanding of the transport of surface passive tracers.

77 In this study, we focus on the North Atlantic Ocean between the equator and 45°N  
 78 to encompass the equatorial and the subtropical gyre dynamics. We combine drifter data  
 79 and a mesoscale eddy database to show that drifters are preferentially trapped into mesoscale  
 80 cyclones compared to anticyclones. Those datasets limited any further investigation so  
 81 we set up a Lagrangian numerical simulation to investigate the underlying mechanisms  
 82 leading to this asymmetry. The paper is organized as follows. Section 2 introduces the  
 83 datasets and numerical framework used in this study. In section 3 we present the obser-  
 84 vational and modelling results and in section 4 we discuss and summarize them.

## 85 2 Data and Methods

### 86 2.1 Observations

87 We used the global daily mesoscale ocean eddy dataset of Faghmous et al. (2015).  
 88 An automatic eddy identification algorithm was used on AVISO’s ‘Delayed Time’, ‘all  
 89 sat merged’ global daily mean sea level anomalies on a 0.25° grid from January 1993 to  
 90 May 2014. The dataset consists in daily anticyclone and cyclone coordinates along with  
 91 some properties, among which we only used the area.

92 We also used a subset of the Global Drifter Program (Niiler, 2001; Lumpkin & Pa-  
 93 zos, 2007) data in the North Atlantic Ocean in the same time window as the eddy database.  
 94 We selected a subset of drifters in 0°-45°N and 110°W-20°E, and then masked the data  
 95 in the Pacific Ocean and the Mediterranean Sea. We retained only drogued drifters to  
 96 discard trajectories that are too much influenced by wind effects (Poulain et al., 2009;  
 97 Grodsky et al., 2011) and inertia (Beron-Vera et al., 2016). The dataset gives 6-hourly  
 98 drifters’ position. Initial positions of drifters are shown in Figure S1a. Commercial ship  
 99 tracks and regions of remarkable dynamics (e.g., Gulf Stream) stand out clearly but we  
 100 checked that the initial distribution of drifters between cyclones and anticyclones was  
 101 unbiased: the total number of drifters is 5811, from which 459 were initially in cyclones  
 102 and 458 in anticyclones (see following paragraph for the attribution of drifters to eddies).

103 We first collocated the drifters and eddies in time, considering they were concomi-  
 104 tant if their positions are given at times closer than 1 h. Drifter trajectories are over-  
 105 all coherent with the eddy polarities: drifters spin clockwise (anticlockwise) in the vicin-  
 106 ity of anticyclones (cyclones). An animation of drifter trajectories and collocated eddy  
 107 positions for year 2000 in the North Atlantic Ocean is available in the Supporting In-  
 108 formation (Movie S1). We considered that a drifter was inside an eddy if the drifter’s  
 109 distance to the eddy center was smaller than the eddy radius. Since the dataset provides  
 110 eddy areas but not eddy contours, we assumed that eddies were circular and derived eddy  
 111 radius from the area. If a drifter appeared to be concomitantly inside two eddies, we con-  
 112 sidered it belonged to the closest eddy.

113      **2.2 Numerical framework**

114      In order to carry out a numerical Lagrangian experiment that mimics the drifters  
 115      spreading, we used the hourly surface velocity and sea surface height (SSH) fields of a  
 116      numerical simulation of ocean currents in the Atlantic (GIGATL6) that is based on the  
 117      Coastal and Regional Ocean Community Model (CROCO, <https://www.croco-ocean.org>,  
 118      developed upon the Regional Oceanic Modelling System, ROMS, Shchepetkin & McWilliams,  
 119      2005). GIGATL6 was designed to solve the hydrostatic and primitive equations on a spher-  
 120      ical grid encompassing the whole Atlantic Ocean (Greenland to Cape Horn) with a nom-  
 121      inal horizontal resolution of 6 km and 50 terrain-following vertical coordinates. The sim-  
 122      ulation thus resolves mesoscale eddies, with at least 5 grid points to represent the first  
 123      baroclinic Rossby radius of deformation ( $R_d$ ) in the region of interest (see Figure 6 in  
 124      Chelton et al., 1998) and typical mesoscale eddy diameter of 2-3  $R_d$  (Figure 11 in Smith,  
 125      2007). The grid bathymetry is from the global SRTM30plus dataset (Becker et al., 2009).  
 126      Initial state and lateral boundary conditions for velocity, SSH, temperature and salin-  
 127      ity are supplied by the Simple Ocean Data Assimilation dataset (Carton & Giese, 2008).  
 128      Atmospheric forcing was supplied at hourly resolution by the Climate Forecast System  
 129      Reanalysis (CFSR, Saha et al., 2010). The simulation started in 2004 and our analy-  
 130      ses were based on one year of outputs in 2009 to ensure that the dynamics was spun up.

131      Daily SSH outputs from GIGATL6 were fed into the py-eddy-tracker software to  
 132      detect mesoscale eddies (<https://py-eddy-tracker.readthedocs.io/en/stable/> Mason et  
 133      al., 2014). In short, py-eddy-tracker sought the outermost closed contours of SSH to iden-  
 134      tify mesoscale eddies. A series of tests was then applied (shape, size, single maximum  
 135      of SSH within a closed contour, etc.) to discard features that were likely not eddies. Once  
 136      the eddies were detected, their closed contours were tracked forward in time. We only  
 137      retained eddies that lived longer than 7 days to ensure their robustness.

138      Hourly surface velocity outputs were used to carry out the Lagrangian dispersion  
 139      experiment using the Pyticles software (Gula et al., 2014). We only used the horizon-  
 140      tal velocity field, i.e., no vertical advection was performed. Synthetic particles were evenly  
 141      released on the model grid with a spacing of  $\approx 1.3$  km between adjacent particles. This  
 142      spacing was chosen to maximise the number of particles while limiting the computational  
 143      cost of the experiment. Particles were passively advected by the surface horizontal cur-  
 144      rents that were bilinearly interpolated in space and linearly interpolated in time at the  
 145      positions of particles with a 6-minute time step.

146      **3 Results**

147      **3.1 Drifters Preferentially Cluster in Mesoscale Cyclones**

148      Figures 1a,b show the total number of cyclones and anticyclones detected in the  
 149      Faghmous et al. (2015) daily dataset, on a regular  $1^\circ \times 1^\circ$  grid (hence, unit is formally  
 150      ‘eddy  $\times$  day’). As expected, a larger number of eddies is found in boundary currents as  
 151      compared to the interior of the subtropical gyre and the equatorial band. There is an  
 152      equipartition of mesoscale cyclones ( $C$ ) and anticyclones ( $AC$ ) throughout the domain,  
 153      with rather patchy binwise relative differences that rarely exceed 50% ( $(\#C - \#AC)/\frac{1}{2}(\#C +$   
 154       $\#AC)$ , Figure 1c). No clear regional pattern emerges and the relative difference over the  
 155      domain is 1.3% in favour of cyclones.

156      We also compare the total surface occupied by cyclones and anticyclones (Figures 1d,e).  
 157      Regional differences stand out in the relative difference map (Figure 1f). The most promi-  
 158      nent one is the Gulf Stream’s extension, whose southern (northern) edge is more cov-  
 159      ered by cyclones (anticyclones). The overall relative difference remains small, with a to-  
 160      tal surface occupied by cyclones that is larger by 4.5%.

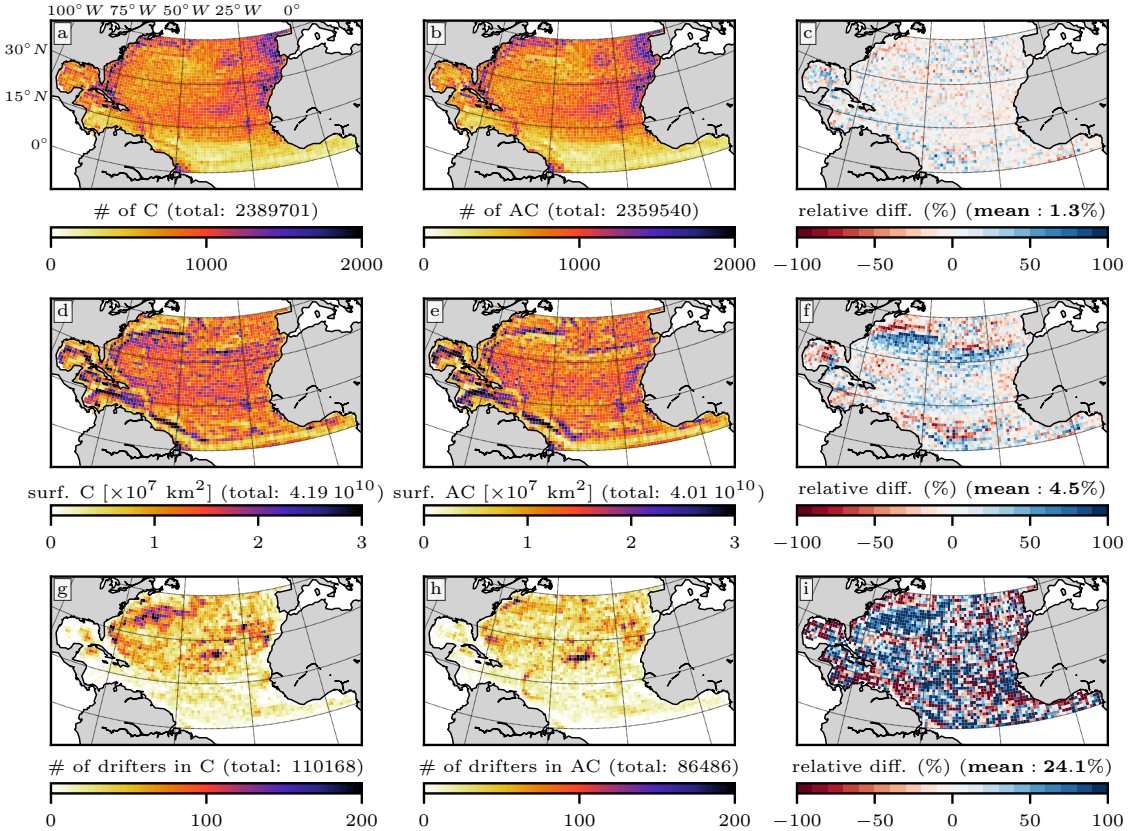


**Figure 1.** Total number of (a) cyclones, (b) anticyclones, and (c) the relative difference of cyclones vs anticyclones in  $1^\circ \times 1^\circ$  bins. Blue (red) areas are dominated by cyclones (anticyclones). Total surface covered by (d) cyclones, (e) anticyclones, and (f) their relative difference. Total number of (g) drifters in cyclones, (h) in anticyclones, and (i) their relative difference. Blue (red) areas indicate that drifters are preferentially trapped into cyclones (anticyclones). Integrated numbers over the area are given above colorbars.

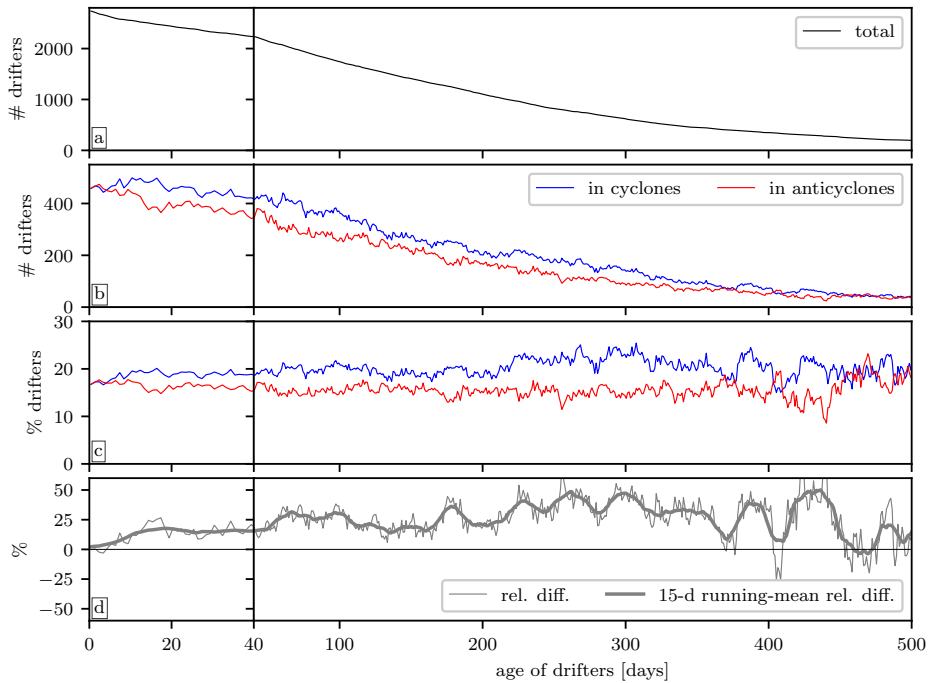


**Figure 2.** Time series relative to the drifters' age. (a) Total number of drifters in the area; (b) number and (c) percentage of drifters in (blue line) cyclones and (red line) anticyclones; (d) (thin gray line) relative difference of drifters in cyclones vs in anticyclones and (bold gray line) its 15-day running mean. Positive means that drifters are preferentially trapped into cyclones.

Figures 1g,h show the number of drifters into cyclones and anticyclones on the same grid. In contrast to the relative equipartition of cyclones and anticyclones, there is a clear preference for drifters to be trapped into cyclones, with pronounced regional trends in the southern edge of the Gulf Stream's extension and within the eastern part of the subtropical gyre (Figure 1i). Overall, mesoscale cyclones contain 24% more drifters than their anticyclonic counterparts. Importantly, this asymmetry cannot be explained by a potential asymmetry in the number of, or area covered by, cyclonic vs anticyclonic eddies. Hence, the trapping asymmetry must be rooted in polarity-dependent kinematics of ocean currents.

Complementary to the static maps described above, we examined the number of drifters into cyclones and anticyclones vis-à-vis of the drifters' age (Figure 2). Time series recall that drifters were equally seeded into cyclones and anticyclones (section 2.1 and Figure 2b). They reveal that the preferred trapping tendency of cyclones builds up within the first  $\sim 20$  days of the drifters' lifecycle and persists over more than 300 days (Figure 2c). Between 20 and 300 days, an average of 20.3% of drifters are found in cyclones vs 15.4% in anticyclones. After about a year, the total number of drifters has significantly decreased (Figure 2a), and the drifters' coverage of the gyre is scarce (Figure S1c,d), hence percentages fluctuate more (Figure 2c). The relative difference between the number of drifters in cyclones and anticyclones reflects the rapidly growing asymmetry, increasing from zero to 15% in 20 days (Figure 2d). Between 20 and 300 days, it fluctuates roughly between 10% and 50%, but overall, within this time period, cyclones contain 27.3% more drifters than anticyclones, consistently with the results that ignored the age of drifters (Figure 1i).

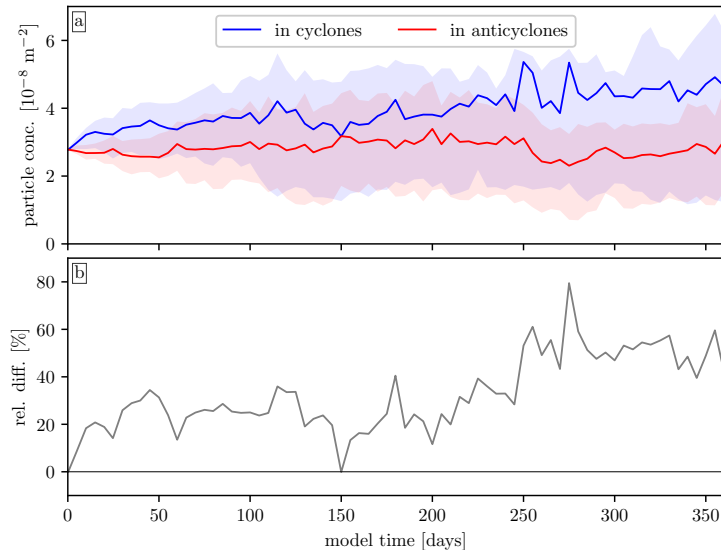


**Figure 3.** Results from the modelling study. (a) Median and quartiles of the concentration of particles in cyclones and anticyclones and (b) the relative difference computed from the median. Positive means an excess of particles into cyclones.

### 3.2 Synthetic Particles Preferentially Cluster in Mesoscale Cyclonic Fronts and Eddies

To further investigate the reasons behind the trapping asymmetry, we set up a basin-scale Lagrangian dispersion experiment using the model outputs of a 6-km resolution numerical model (section 2.2). Figure S2 (Supporting Information) shows a snapshot of particles' position, surface relative vorticity and eddy contours. We compute the concentration of particles in eddies for each individual as the number of particles divided by the eddy surface (output by py-eddy-tracker). Then, we derive statistics for each eddy polarity every 5 days. Figure 3a shows time series of the median and quartiles of particle concentration in cyclones and anticyclones. It thus gives an overview of the distribution of particle concentration. The particle concentration in cyclones and anticyclones is strictly equal at the release. The relative difference builds up within the first  $\approx 30$  days and fluctuates around 20% between 30 and 200 days before increasing and plateauing around 40% (Figure 3b). Reasons for this stepwise evolution remain unclear. However, the modelling results are overall consistent with the observations and confirm that mesoscale cyclones trap more surface buoyant material than anticyclones.

Visual inspection of particles and surface vorticity fields suggests two important points (Supporting Information Movie S2). First, particles cluster preferentially in cyclonic areas, regardless of the type of structures, i.e., fronts or eddies. Second, it suggests that the clustering of particles occurs prior to the detection of eddies. Specifically, we routinely observe clusterings of particles in cyclonic fronts before the latter roll up into mesoscale cyclones subsequently detected by the algorithm.

We carried out several diagnostics to confirm those visual impressions. Inspired by Balwada et al. (2021), we examine the mean particle concentration as a function of vertical vorticity ( $\zeta = \partial_x v - \partial_y u$ , with  $(u, v)$  the horizontal velocity in the  $(x, y)$ , i.e., zonal and meridional, coordinate system) and strain ( $\sigma = \sqrt{\sigma_n^2 + \sigma_s^2}$ , with  $\sigma_n = \partial_x u - \partial_y v$  and  $\sigma_s = \partial_x v + \partial_y u$ ). Figure 4b strongly supports the first observation. Indeed, particle concentration is rather homogeneous ( $\approx 1-2 \times 10^{-8} \text{ m}^{-2}$ ) in most of the vorticity-

212 strain domain but a clear two-to-three times increase in concentration (up to  $6 \times 10^{-8} \text{ m}^{-2}$ )  
 213 is found approaching and past the  $\sigma = \zeta$  line on the cyclonic side ( $\zeta > 0$ ). This line  
 214 materializes cyclonic fronts, whereas the area below ( $\zeta > \sigma$ ) is dominated by more ma-  
 215 terially coherent spinning structures (Balwada et al., 2021).

216 The second point was tested by identifying particles belonging to an eddy at its  
 217 first detection and tracking them backward in time to get insights on the trapping sce-  
 218 nario. We specifically monitored the flow vorticity and divergence ( $\delta = \partial_x u + \partial_y v$ ) in-  
 219 terpolated at the particles' position (Figures 4c,d). Time series reveal that most parti-  
 220 cles acquire the polarity of the eddy they are going to get trapped in between 5 and 15  
 221 days before the eddy is actually detected. Remarkably, 5 days prior to the eddy detec-  
 222 tion, more than half of the particles already have the polarity of the eddy they are go-  
 223 ing to be trapped in (the envelop of quartiles does not cross the zero line, Figure 4c).  
 224 Note that this tendency is more pronounced for cyclonic flows that feature larger vor-  
 225 ticity. Furthermore,  $\delta/f$  is negative for most particles – they are by definition attracted  
 226 in convergence zones ( $\delta/f < 0$ ) – and does not show any difference for the cyclonic and  
 227 anticyclonic cases until  $\approx 10$  days before the eddy detection (Figure 4d). Around this  
 228 time, particles that are going to be trapped into cyclones see a negative divergence that  
 229 is roughly twice as large as the ones that are going to be trapped into anticyclones. This  
 230 emphasizes the enhanced clustering of particles in cyclonic regions before the actual de-  
 231 tection of the mesoscale cyclones they are going to be trapped in.

## 232 4 Summary and Discussion

233 Our study sheds light on the hitherto undocumented asymmetric role of mesoscale  
 234 eddies to cluster surface buoyant material. Combining surface drifters with a mesoscale  
 235 eddy database, we demonstrated that cyclones cluster roughly 24% more drifters than  
 236 anticyclones. A numerical Lagrangian experiment using a mesoscale-resolving model re-  
 237 produces this asymmetry and helped us to gain insight into the trapping scenario, which  
 238 is as follows. Statistically, particles are more concentrated in cyclonic regions, includ-  
 239 ing fronts and eddies. For particles that end up being trapped in eddies, a backward track-  
 240 ing indicates that they tend to acquire the eddies' polarity while the eddy is formed, which  
 241 corresponds to a few days before it is actually detected. This preconditioning is more  
 242 prominent in cyclonic flows and, added up to the background higher concentration of par-  
 243 ticles in cyclonic regions, qualitatively explains the asymmetry in particle concentration  
 244 between mesoscale cyclonic and anticyclonic eddies. Note that we extended the obser-  
 245 vational analysis to the whole Atlantic Ocean and obtained quantitatively similar results.

246 At first sight, the clustering asymmetry is unanticipated. Indeed, while in submesoscale-  
 247 dominated regimes, clustering of material in cyclonic regions is documented and ratio-  
 248 nalised (D'Asaro et al., 2018; Berta et al., 2020; Balwada et al., 2021; Esposito et al.,  
 249 2021), such an asymmetry is unexpected at the mesoscale – see the introductory review  
 250 of literature in section 1. Our model resolution formally allows an accurate representa-  
 251 tion of mesoscales but hardly permits submesoscales. This is *a posteriori* diagnosed through  
 252 the joint probability density function of vorticity and strain, which is roughly symmet-  
 253 ric relative to vorticity, while hinting that ageostrophic currents ( $|\zeta/f| > 1$ ) can develop  
 254 (Figure 4a). We thus hypothesise that the rare (PDF  $< 10^{-2} \%$ ) ageostrophic fronto-  
 255 genesis that occurs in the model is instrumental at clustering particles in cyclonic fronts  
 256 and preconditioning the higher concentration in cyclonic eddies. Indeed, the secondary  
 257 circulation associated with those fronts is key to drive a convergence of material in cy-  
 258 clonic regions (Barkan et al., 2019). Note that this preconditioning is also consistent with  
 259 the findings of Zhang and Qiu (2018) that showed that ageostrophic motions within mesoscale  
 260 eddies are intensified at the beginning of their lifecycle.

261 An examination of the literature on physical-biological-biogeochemical interactions  
 262 at the mesoscale could not shed us some light over any clear mechanism that could lead

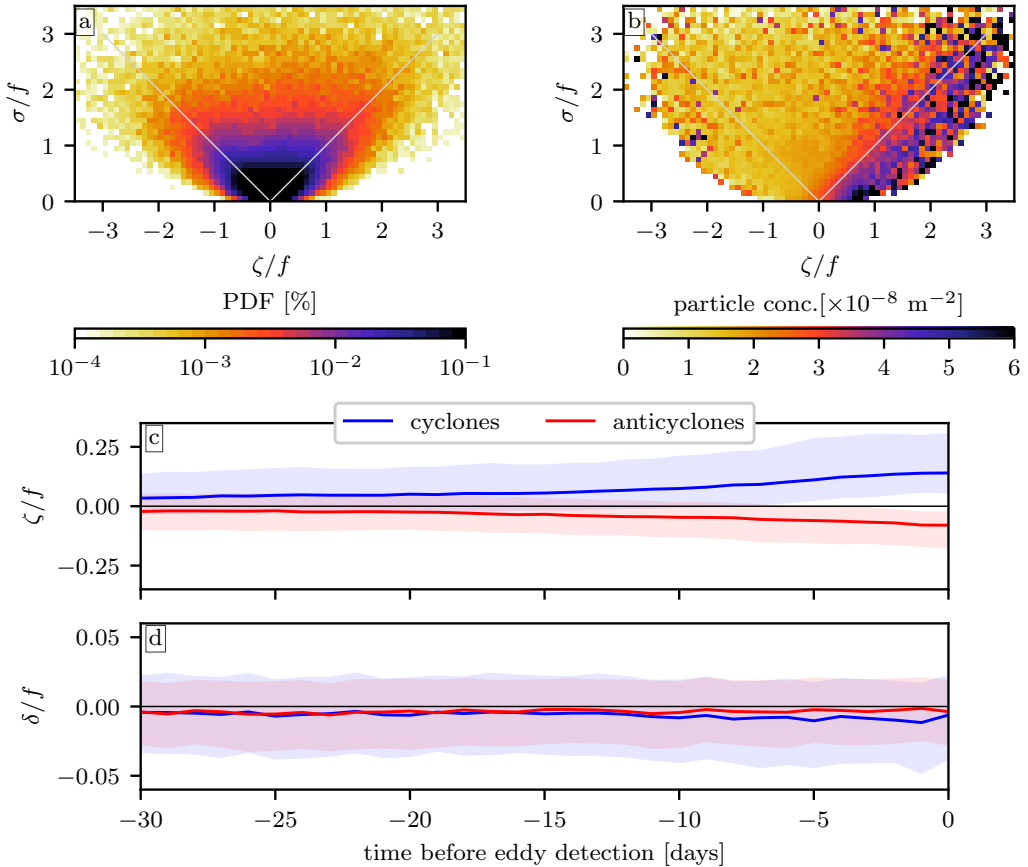


**Figure 4.** Results from the modelling study. (a) Joint Probability Density Function of relative vorticity  $\zeta/f$  and strain  $\sigma/f$ , both non-dimensionalised by the local Coriolis frequency. (b) Mean particle concentration per bin in vorticity-strain space (bin width is 0.1). (a) and (b) are averaged over 16 frames covering the whole domain and evenly spaced in time between 10 days and 100 days of simulation. Grey lines represent  $\sigma = |\zeta|$ . Model (c) vorticity  $\zeta/f$  and (d) divergence  $\delta/f$  (median and quartiles), both non-dimensionalised by the local Coriolis frequency, seen by particles before they are trapped into cyclones (blue) and anticyclones (red).

263 to surface clustering. Higher chlorophyll concentrations are consistently found in anti-  
 264 cyclones as compared to cyclones, which has to be explained by an enhanced net upward  
 265 transport of nutrients (observations are reviewed in McGillicuddy Jr, 2016). Several mech-  
 266 anisms are invoked to explain the enhancement of vertical velocities in mesoscale eddies  
 267 (e.g. Martin & Richards, 2001) but only two have asymmetrical effects in cyclones and  
 268 anticyclones (eddy pumping and Ekman pumping, reviewed in the introduction, based  
 269 on McGillicuddy Jr, 2016). Systematically quantifying the importance of those mech-  
 270 anisms is arduous, since eddy pumping intrinsically depends on the generation mecha-  
 271 nism, and Ekman pumping depends on wind stress and eddy velocity, both spanning wide  
 272 ranges of values. Nonetheless, we claim that these two mechanisms do not play a sig-  
 273 nificant role in the asymmetry we observe here. Eddy pumping should lead to a diver-  
 274 gence of material in cyclones during their formation, which is opposite to our observa-  
 275 tions. Ekman pumping could contribute to the increased convergence in cyclones. How-  
 276 ever, clustering happens prior to the eddy detection and the asymmetry does not change  
 277 significantly after the eddies are formed, which lead us to consider Ekman pumping as  
 278 a second-order mechanism to explain the flow convergence in mesoscale cyclones.

279 Also, note that the literature review of van Sebille et al. (2020) on the physics in-  
 280 volved in the dispersion of floating debris only reports one case where plastic concentra-  
 281 tion was higher in an anticyclone as compared to a neighbouring cyclone (Brach et al.,  
 282 2018). Clearly, this result needs to be statistically tested.

283 Our study has several limitations. Probably the most important is about the eddy  
 284 detection and tracking method, regarding both the observational and modelling meth-  
 285 ods and results. Some recent articles highlighted the inherent limitations of tracking mesoscale  
 286 eddies through altimetry and/or with SSH-based techniques (e.g., Amores et al., 2018;  
 287 Stegner et al., 2021). In addition, the classic vision of materially-coherent mesoscale ed-  
 288 dries has been questioned over the last decade, emphasising the leakiness of such struc-  
 289 tures (e.g., Cetina-Heredia et al., 2019; Liu et al., 2019). Furthermore, as the resolu-  
 290 tion of numerical models and observations increases, emerging submesoscale three-dimensional  
 291 circulations seem to play a preponderant role in shaping material patterns in the sur-  
 292 face layers (e.g., Lévy et al., 2018; Uchida et al., 2019). These questions will be addressed  
 293 in future work.

#### 294 Acknowledgments

295 J.G. gratefully acknowledges support from the French National Agency for Research (ANR)  
 296 through the project DEEPER (ANR-19-CE01-0002-01). J.G. acknowledges PRACE and  
 297 GENCI for awarding access to HPC resources Joliot-Curie Rome and SKL from GENCI-  
 298 TGCC (Grants 2020-A0090112051, 2019gch0401 and PRACE project 2018194735) and  
 299 HPC facilities DATARMOR of “Pôle de Calcul Intensif pour la Mer” at Ifremer (Brest,  
 300 France). The authors thank Gildas Cambon and Sébastien Theetthen for their contri-  
 301 bution in the development of the realistic numerical simulation GIGATL6. Information  
 302 about the simulations can be found at <https://doi.org/10.5281/zenodo.4948523>. We down-  
 303 loaded the eddy database from <https://datadryad.org/stash/dataset/doi:10.5061/dryad.gp40h> and the Global Drifter Program data from <https://www.aoml.noaa.gov/phod/gdp/interpolated/data/subset.php>.

#### 306 References

- 307 Abernathey, R., & Haller, G. (2018). Transport by Lagrangian vortices in the East-  
 308 ern Pacific. *Journal of Physical Oceanography*, 48(3), 667–685. doi: 10.1175/  
 309 JPO-D-17-0102.1
- 310 Amores, A., Jordà, G., Arsouze, T., & Le Sommer, J. (2018). Up to what extent  
 311 can we characterize ocean eddies using present-day gridded altimetric prod-  
 312 ucts? *Journal of Geophysical Research Oceans*, 123(10), 7220–7236. doi:

- 313 10.1029/2018JC014140
- 314 Balwada, D., Xiao, Q., Smith, S., Abernathey, R., & Gray, A. R. (2021). Vertical  
315 fluxes conditioned on vorticity and strain reveal submesoscale venti-  
316 lation. *Journal of Physical Oceanography*, 51, 2883–2901. doi: 10.1175/  
317 JPO-D-21-0016.1
- 318 Barkan, R., Molemaker, M. J., Srinivasan, K., McWilliams, J. C., & D'Asaro,  
319 E. A. (2019). The role of horizontal divergence in submesoscale fron-  
320 togenesis. *Journal of Physical Oceanography*, 49(6), 1593–1618. doi:  
321 10.1175/JPO-D-18-0162.1
- 322 Becker, J., Sandwell, D., Smith, W., Braud, J., Binder, B., Depner, J., ... oth-  
323 ers (2009). Global bathymetry and elevation data at 30 arc seconds  
324 resolution: SRTM30\_PLUS. *Marine Geodesy*, 32(4), 355–371. doi:  
325 10.1080/01490410903297766
- 326 Beron-Vera, F. J., Olascoaga, M. J., & Lumpkin, R. (2016). Inertia-induced ac-  
327 cumulation of flotsam in the subtropical gyres. *Geophysical Research Letters*,  
328 43(23), 12–228. doi: 10.1002/2016GL071443
- 329 Berta, M., Griffa, A., Haza, A., Horstmann, J., Huntley, H., Ibrahim, R., ... Poje,  
330 A. (2020). Submesoscale kinematic properties in summer and winter surface  
331 flows in the Northern Gulf of Mexico. *Journal of Geophysical Research Oceans*,  
332 125(10), e2020JC016085. doi: 10.1029/2020JC016085
- 333 Brach, L., Deixonne, P., Bernard, M.-F., Durand, E., Desjean, M.-C., Perez, E., ...  
334 Ter Halle, A. (2018). Anticyclonic eddies increase accumulation of microplas-  
335 tic in the North Atlantic subtropical gyre. *Marine pollution bulletin*, 126,  
336 191–196. doi: 10.1016/j.marpolbul.2017.10.077
- 337 Buckingham, C. E., Naveira Garabato, A. C., Thompson, A. F., Brannigan, L.,  
338 Lazar, A., Marshall, D. P., ... Belcher, S. E. (2016). Seasonality of sub-  
339 mesoscale flows in the ocean surface boundary layer. *Geophysical Research  
340 Letters*, 43(5), 2118–2126. doi: 10.1002/2016GL068009
- 341 Capet, X., Klein, P., Hua, B. L., Lapeyre, G., & McWilliams, J. C. (2008). Surface  
342 kinetic energy transfer in surface quasi-geostrophic flows. *Journal of Fluid Me-  
343 chanics*, 604, 165–174. doi: 10.1017/S0022112008001110
- 344 Carton, J., & Giese, B. (2008). A reanalysis of ocean climate using Simple Ocean  
345 Data Assimilation (SODA). *Monthly Weather Review*, 136(8), 2999–3017. doi:  
346 10.1175/2007MWR1978.1
- 347 Cetina-Heredia, P., Roughan, M., van Sebille, E., Keating, S., & Brassington, G. B.  
348 (2019). Retention and leakage of water by mesoscale eddies in the East Aus-  
349 tralian Current system. *Journal of Geophysical Research Oceans*, 124(4),  
350 2485–2500. doi: 10.1029/2018JC014482
- 351 Chelton, D. B., DeSzoeke, R. A., Schlax, M. G., El Naggar, K., & Siwertz,  
352 N. (1998). Geographical variability of the first baroclinic Rossby ra-  
353 dius of deformation. *J. Phys. Oceanogr.*, 28(3), 433–460. doi: 10.1175/  
354 1520-0485(1998)028<0433:GVOTFB>2.0.CO;2
- 355 Chelton, D. B., Schlax, M. G., & Samelson, R. M. (2011). Global observations of  
356 nonlinear mesoscale eddies. *Prog. Oceanogr.*, 91(2), 167–216. doi: 10.1016/j  
357 .pocean.2011.01.002
- 358 D'Asaro, E. A., Shcherbina, A. Y., Klymak, J. M., Molemaker, J., Novelli, G.,  
359 Guigand, C. M., ... others (2018). Ocean convergence and the dispersion  
360 of flotsam. *Proceedings of the National Academy of Sciences*, 115(6), 1162–  
361 1167. doi: 10.1073/pnas.1718453115
- 362 Esposito, G., Berta, M., Centurioni, L., Lodise, J., Ozgokmen, T., Poulain, P.-M.,  
363 & Griffa, A. (2021). Submesoscale vorticity and divergence in the Alboran  
364 Sea: scale and depth dependence. *Frontiers in Marine Science*, 8, 843. doi:  
365 10.3389/fmars.2021.678304
- 366 Faghmous, J. H., Frenger, I., Yao, Y., Warmka, R., Lindell, A., & Kumar, V. (2015).  
367 A daily global mesoscale ocean eddy dataset from satellite altimetry. *Scientific*

- 368                   *data*, 2(1), 1–16. doi: 10.1038/sdata.2015.28
- 369     Flierl, G., & McGillicuddy, D. J. (2002). *Mesoscale and submesoscale physical-*  
 370                   *biological interactions* (Vol. 12; A. Robinson, J. McCarthy, & B. Rothschild,  
 371                   Eds.). Wiley New York.
- 372     Gaube, P., Chelton, D. B., Samelson, R. M., Schlax, M. G., & O'Neill, L. W. (2015).  
 373                   Satellite observations of mesoscale eddy-induced Ekman pumping. *Journal of*  
 374                   *Physical Oceanography*, 45(1), 104–132. doi: 10.1175/JPO-D-14-0032.1
- 375     Grodsky, S. A., Lumpkin, R., & Carton, J. A. (2011). Spurious trends in global  
 376                   surface drifter currents. *Geophysical Research Letters*, 38(10). doi: 10.1029/  
 377                   2011GL047393
- 378     Gula, J., Molemaker, M. J., & McWilliams, J. C. (2014). Submesoscale cold fil-  
 379                   aments in the Gulf Stream. *Journal of Physical Oceanography*, 44(10), 2617–  
 380                   2643. doi: 10.1175/JPO-D-14-0029.1
- 381     Lévy, M., Franks, P. J., & Smith, K. S. (2018). The role of submesoscale currents  
 382                   in structuring marine ecosystems. *Nature Commun.*, 9(1), 4758. doi: 10.1038/  
 383                   s41467-018-07059-3
- 384     Liu, T., Abernathey, R., Sinha, A., & Chen, D. (2019). Quantifying Eulerian eddy  
 385                   leakiness in an idealized model. *Journal of Geophysical Research Oceans*,  
 386                   124(12), 8869–8886. doi: 10.1029/2019JC015576
- 387     Lumpkin, R., & Pazos, M. (2007). *Measuring surface currents with surface velocity*  
 388                   *program drifters: the instrument, its data, and some recent results* (A. Griffa,  
 389                   A. Kirwan Jr, A. J. Mariano, T. Özgökmen, & H. T. Rossby, Eds.). Cambridge  
 390                   University Press.
- 391     Martin, A. P., & Richards, K. J. (2001). Mechanisms for vertical nutrient transport  
 392                   within a North Atlantic mesoscale eddy. *Deep Sea Research Part II*, 48(4–5),  
 393                   757–773. doi: 10.1016/S0967-0645(00)00096-5
- 394     Mason, E., Pascual, A., & McWilliams, J. C. (2014). A new sea surface height-based  
 395                   code for oceanic mesoscale eddy tracking. *Journal of Atmospheric and Oceanic*  
 396                   *Technology*, 31(5), 1181–1188. doi: 10.1175/JTECH-D-14-00019.1
- 397     McGillicuddy Jr, D. J. (2016). Mechanisms of physical-biological-biogeochemical in-  
 398                   teraction at the oceanic mesoscale. *Annual Review of Marine Science*, 8, 125–  
 399                   159. doi: 10.1146/annurev-marine-010814-015606
- 400     McWilliams, J. C. (2008). The nature and consequences of oceanic eddies. *Ocean*  
 401                   *modeling in an eddying regime*, 177, 5–15. doi: 10.1029/177GM03
- 402     Niiler, P. (2001). The world ocean surface circulation. In *International geophysics*  
 403                   (Vol. 77, pp. 193–204). doi: 10.1016/S0074-6142(01)80119-4
- 404     Penven, P., Halo, I., Pous, S., & Marié, L. (2014). Cyclogeostrophic balance in the  
 405                   Mozambique Channel. *Journal of Geophysical Research Oceans*, 119(2), 1054–  
 406                   1067. doi: 10.1002/2013JC009528
- 407     Polvani, L. M., McWilliams, J. C., Spall, M. A., & Ford, R. (1994). The coher-  
 408                   ent structures of shallow-water turbulence: Deformation-radius effects, cy-  
 409                   clone/anticyclone asymmetry and gravity-wave generation. *Chaos*, 4(2),  
 410                   177–186.
- 411     Poulain, P.-M., Gerin, R., Mauri, E., & Pennel, R. (2009). Wind effects on drogued  
 412                   and undrogued drifters in the eastern Mediterranean. *Journal of Atmospheric*  
 413                   *and Oceanic Technology*, 26(6), 1144–1156. doi: 10.1175/2008JTECHO618.1
- 414     Roullet, G., & Klein, P. (2010). Cyclone-anticyclone asymmetry in geophysical tur-  
 415                   bulence. *Physical review letters*, 104(21), 218501. doi: 10.1103/PhysRevLett  
 416                   .104.218501
- 417     Rudnick, D. L. (2001). On the skewness of vorticity in the upper ocean. *Geophysical*  
 418                   *Research Letters*, 28(10), 2045–2048. doi: 10.1029/2000GL012265
- 419     Saha, S., Moorthi, S., Pan, H.-L., Wu, X., Wang, J., Nadiga, S., ... others (2010).  
 420                   The NCEP climate forecast system reanalysis. *Bulletin of the American Meteo-*  
 421                   *rological Society*, 91(8), 1015–1058. doi: 10.1175/2010BAMS3001.1
- 422     Shchepetkin, A., & McWilliams, J. (2005). The regional oceanic modeling system

- 423 (ROMS): a split-explicit, free-surface, topography-following-coordinate oceanic  
424 model. *Ocean Modell.*, 9(4), 347–404. doi: 10.1016/j.ocemod.2004.08.002
- 425 Shcherbina, A. Y., D’Asaro, E. A., Lee, C. M., Klymak, J. M., Molemaker, M. J., &  
426 McWilliams, J. C. (2013). Statistics of vertical vorticity, divergence, and strain  
427 in a developed submesoscale turbulence field. *Geophys. Res. Lett.*, 40(17),  
428 4706–4711. doi: 10.1002/grl.50919
- 429 Smith, K. S. (2007). The geography of linear baroclinic instability in Earth’s oceans.  
430 *J. Mar. Res.*, 65(5), 655–683. doi: 10.1357/002224007783649484
- 431 Stegner, A., Le Vu, B., Dumas, F., Ghannami, M. A., Nicolle, A., Durand, C., &  
432 Faugere, Y. (2021). Cyclone-anticyclone asymmetry of eddy detection on  
433 gridded altimetry product in the Mediterranean Sea. *Journal of Geophysical  
434 Research Oceans*, 126(9), e2021JC017475. doi: 10.1029/2021JC017475
- 435 Uchida, T., Balwada, D., Abernathey, R., McKinley, G., Smith, S., & Levy, M.  
436 (2019). The contribution of submesoscale over mesoscale eddy iron transport  
437 in the open Southern Ocean. *Journal of Advances in Modeling Earth Systems*,  
438 11(12), 3934–3958. doi: 10.1029/2019MS001805
- 439 Vallis, G. K. (2006). *Atmospheric and oceanic fluid dynamics: fundamentals and  
440 large-scale circulation*. Cambridge University Press.
- 441 van Sebille, E., Aliani, S., Law, K. L., Maximenko, N., Alsina, J. M., Bagaev, A.,  
442 ... others (2020). The physical oceanography of the transport of float-  
443 ing marine debris. *Environmental Research Letters*, 15(2), 023003. doi:  
444 10.1088/1748-9326/ab6d7d
- 445 Zhang, Z., & Qiu, B. (2018). Evolution of submesoscale ageostrophic motions  
446 through the life cycle of oceanic mesoscale eddies. *Geophysical Research Let-  
447 ters*, 45(21), 11–847. doi: 10.1029/2018GL080399
- 448 Zhang, Z., Wang, W., & Qiu, B. (2014). Oceanic mass transport by mesoscale ed-  
449 dies. *Science*, 345(6194), 322–324. doi: 10.1126/science.1249770